CHEMISTRY & SUSTAINABILITY
CHEMSUSCHEM
ENERGY & MATERIALS

Accepted Article

Title: Mellitic Triimides Showing Three One-Electron Redox Reactions with Increased Redox Potential as New Electrode Materials for Li-ion Batteries

Authors: Dong Joo Min, Kyu Nam Lee, Soo Young Park, and Ji Eon Kwon

To be cited as: *ChemSusChem* 10.1002/cssc.202000180

Link to VoR: http://dx.doi.org/10.1002/cssc.202000180

A Journal of
ChemPubSoc Europe

WILEY-VCH www.chemsuschem.org

Mellitic Triimides Showing Three One-Electron Redox Reactions with Increased Redox Potential as New Electrode Materials for Li-ion Batteries

Dong Joo Min, Kyunam Lee, Soo Young Park,* and Ji Eon Kwon*

Research Institute of Advanced Materials (RIAM), Department of Materials Science and Engineering, Seoul National University, 1 Gwanak-ro, Gwanak-gu, Seoul 08826, Republic of Korea

Abstract

The mellitic triimide (MTI) bearing three imide groups on a benzene core with C3 symmetry is proposed as a new building block for organic electrode materials in lithium-ion batteries. It is anticipated that MTI delivers a higher theoretical specific capacity up to 282 mAh g^{-1} with more increased reduction potentials than the well-known pyromellitic diimide (PyDI) building block bearing two imide groups because the additional imide group can accept one more electron and provide the electron-withdrawing effect. A model compound, ethyl-substituted mellitic triimide (ETTI), shows well distinguished and reversible three one-electron redox reactions at -0.97, -1.62, and -2.34 V vs. Ag/Ag^+ in 0.1 M tetrabutylammonium hexafluorophosphate (TBAHFP) electrolyte, but the redox potentials are much more increased in 2 M lithium bis(trifluoromethanesulfonyl)imide (LiTFSI) electrolyte, which are -0.60 V, -0.86 V, and -1.42 V vs. Ag/Ag^+. The DFT calculation reveals that the unique C3 symmetric structural design leads to the more elevated reduction potential of MTI in the Li-based electrolyte by formation of a stable 7-membered ring with a Li-ion and the two carbonyl oxygen atoms of the adjacent imide groups. In a Li-ion coin cell, the ETTI electrode delivers a specific capacity of 176 mAh g^{-1}, corresponding 81% of capacity utilization, with clear three voltage plateaus. It should be noted that the elevated average discharge voltage (2.41 V vs Li/Li^+) of ETTI allows it to deliver one of the highest specific energy (421 Wh kg^{-1}) among reported diimide (DI)-based electrode materials. Finally, its redox mechanism is investigated by ex-situ FT-IR measurements and DFT calculation.

Introduction

Lithium-ion batteries (LIBs) based on inorganic metal oxide cathodes have met with great success in a small battery market and have become essential components for portable electronic devices such as mobile phones and laptop computers.[1-2] Recently, along with the development of the more electricity-drawing electronic devices and renewable-energy power plants requiring large-scale energy storages, there is an increasing demand for innovations in battery technologies.[3-4] However, the performance of conventional metal oxide electrodes have reached their theoretical limit, and in addition, the price of heavy metal elements essential for producing them such as Cobalt has been steeply rising because of the limited reserves.[5] In such a situation, organic electrodes based on abundant and inexpensive elements have received growing attention due to their many advantages such as high theoretical specific capacity, easy chemical tunability, and eco-friendliness.[6-8]

To date, various kinds of organic electrodes have been reported including nitroxides,[9-10] organosulfurs,[11-12] tetrazines,[13] carboxylates,[14-16] quinones,[17-19] and imides.[20-23] In particular, aromatic diimides (DIs) have shown great promise as cathode materials for secondary batteries with high capacity, outstanding cycle stability, and good rate performance. For example, DIs-bearing small molecules,[24] oligomers,[25] polymers,[26-29] and carbon composites[30] have been reported for electrodes in various metal-ion batteries including Li-,[24-25, 30] Na-,[26] K-,[27] Mg-,[28] and Ca-ion.[29] Theoretically, an aromatic imide bearing two carbonyl groups should be reduced by two electrons because each carbonyl group can accept one electron by the reduction. However, in practice, it is well known that only one of the two carbonyls in the imide reversibly receive an electron and bind a metal ion to form a metal enolate during a discharge process (Scheme 1b).[31-35] The additional reduction of the other carbonyl group in the imide would lead to decomposition of the molecule. Hence, reasonably high theoretical specific capacities can be expected from the DIs utilizing two electrons, which are up to 248 mAh g^{-1} for pyromellitic diimide (PyDI), 201 mAh g^{-1} for naphthalene diimide (NDI), and 137 mAh g^{-1} for perylene diimide (PDI), respectively (Scheme 1a, b). Practically, Renault et al.[36] and Shi et al.[37] achieved 220 and 200 mAh g^{-1} of specific capacities using a dilithium salt of PyDI and a non-substituted NDI, respectively. Nevertheless, considering their rather low redox potential (< 2.5 V *vs.* Li/Li^+), it is still necessary to further improve their energy density.

Since the energy density of a cell is the product of cell voltage and capacity, to achieve high energy density, both redox potential and specific capacity of cathode materials should be increased simultaneously. First, the theoretical capacity of an electrode material can be calculated as

$$C_{theo} = \frac{nF}{3.6M}, \qquad (1)$$

where C_{theo} is the theoretical specific capacity (mAh g^{-1}), n is the number of electrons involved redox reactions of

10.1002/cssc.202000180

a molecule, *F* is Faraday constant (C mol^{-1}), and *M* is the molecular weight (g mol^{-1}).[31] Therefore, according to Equation (1), higher theoretical capacity can be achieved by introducing more redox centers into a molecule to induce multi-electron reactions while minimizing its molecular weight.

On the other hand, the redox potential of organic materials can easily be tuned by introducing electron-withdrawing or electron-donating substituents.[20, 38-39] Such substituents typically affect the frontier molecular orbital (FMO) levels of organic molecules, which are closely related to their electron affinity (EA) and ionization potential (IP), leading to a change in their redox potential. For example, Vadehra et al.[39] and Banda et al.[20] achieved 0.4–0.5 V elevation of the first reduction potential of NDI and PDI by introducing CN groups, respectively. This is attributed to that the strong electron-withdrawing nature of the CN substituents stabilized the lowest unoccupied molecular orbital (LUMO) level of NDI and PDI and thereby increased their EA. However, the substitution of such redox-inactive groups naturally increased their molecular weight, resulting in a significant reduction of their theoretical specific capacity. Therefore, to achieve a high energy density of DIs, a novel approach that can elevate the redox potential while minimizing the increment of the molecular weight caused by substitution is highly demanded.

Herein, we propose mellitic triimide (MTI) bearing three imide groups with C3 symmetry as a new building block for organic electrode materials with large specific capacity and high energy density (Scheme 1). MTI has one more imide redox center than PyDI, which is the smallest DI, on the identical benzene core. Therefore, it can undergo three one-electron reductions while the molecular weight of its redox-inactive portion is just identical to that of PyDI, which lends it much improved theoretical specific capacity up to 282 mAh g^{-1}. Furthermore, it is also anticipated that the reduction potential of MTI is higher than PyDI because the LUMO level of MTI should be more stabilized by the electron-withdrawing effect of the additional imide group. In this study, to evaluate potential applicability of MTI as a building block for electrode materials, we designed and synthesized two model compounds, 2,5,8-triethyl-1H-dipyrrolo[3,4-e:3',4'-g]isoindole-1,3,4,6,7,9(2H,5H,8H)-hexaone (ETTI) and 2,5,8-tribenzyl-1H-dipyrrolo[3,4-e:3',4'-g]isoindole-1,3,4,6,7,9(2H,5H,8H)-hexaone (BZTI) (Figure 1a), possessing ethyl and benzyl side chains, respectively. For comparative studies, we also synthesized a PyDI-based model compound 2,6-diethylpyrrolo[3,4-f]isoindole-1,3,5,7(2H,6H)-tetraone (ETDI). The electrochemical properties of the compounds were thoroughly studied by cyclic voltammetry (CV) and computational calculation using density functional theory (DFT). Interestingly, the additional elevation of the reduction potential of the MTIs was observed in an electrolyte containing Li-ion salts than in a tetrabutylammonium-based electrolyte, which is due to the fact that the interaction between the inserted Li-ion and the adjacent two imide groups of the MTI molecules forming a stable heptagonal ring by reduction. Finally, we evaluated their potential applicability as cathode materials in Li-ion coin cells and investigated their charge/discharge mechanism using ex-situ Fourier-transform infrared (FT-IR) spectroscopy.

Results and discussion

Materials design and synthesis

The MTIs were synthesized by a very simple two-step procedure: formation of triammonium salt of mellitic acid with primary amines, followed by solid-state thermal dehydration.[40-41] At first, we attempted to synthesize an MTI bearing three methyl groups at the N-positions as the simplest MTI molecule. However, it was hard to be obtained due to the low boiling point of methyl amine (B.P = −6 °C). In contrast, ETTI (C_{theo} = 217 mAh g^{-1}) was successfully synthesized using ethyl amine (B.P = 16.6 °C) with a good yield (Figure 1a). As a control PyDI compound, we also synthesized ETDI (C_{theo} = 197 mAh g^{-1}) bearing two ethyl groups by dehydration reaction with pyromellitic dianhydride and ethyl amine in dimethylformamide (DMF) solution. The chemical structures of the synthesized compounds were fully characterized by ^{1}H- and ^{13}C-NMR, and high-resolution mass spectroscopy (HR-MS). The detailed synthesis procedures and characterization data are fully described in the Experimental section.

Meanwhile, we carried out DFT calculations of the designed imide materials using B3LYP functional with 6-311+G(d,p) basis set. To reduce the calculation cost, we used MTI and PyDI molecules bearing methyl side chains instead of the ethyl groups for the calculation because the length of side chains barely affects the electronic structure of the molecules. As expected, the calculation results in gas phase show that the LUMO level of ETTI (E_{LUMO} = -3.66 eV) is more stabilized than ETDI (E_{LUMO} = -3.53 eV) (Figure 1b) due to the electron-withdrawing effect of the additional imide group in ETTI, implying higher first reduction potential of MTI than PyDI.

Electrochemical properties

The electrochemical properties of the imides were investigated in acetonitrile solutions with 0.1 M tetrabutylammonium hexafluorophosphate (TBAHFP) as a supporting electrolyte and an Ag wire in 0.01 M $AgNO_3$ solution as a reference electrode. A CV scan of ETDI shows two reversible one-electron redox reactions, and the reduction potentials are -1.16 V (${}^1E_{1/2,\ \text{ETDI-TBA}}$) and -1.76 V (${}^2E_{1/2,\ \text{ETDI-TBA}}$) vs. Ag/Ag$^+$, respectively, at a scan rate of 50 mV s^{-1} (Figure 2a). In contrast, ETTI shows three reversible one-electron redox reactions, and the reduction potentials are -0.97 V (${}^1E_{1/2,\ \text{ETTI-TBA}}$), -1.62 V (${}^2E_{1/2,\ \text{ETTI-TBA}}$), and -2.34 V (${}^3E_{1/2,\ \text{ETTI-TBA}}$) vs. Ag/Ag$^+$, respectively (Figure 2b). It should be noted that the first and second reduction potentials of ETTI are higher than those of ETDI by 0.19 (${}^1E_{1/2,\ \text{ETTI-TBA}} - {}^1E_{1/2,\ \text{ETDI-TBA}}$) and 0.14 V (${}^2E_{1/2,\ \text{ETTI-TBA}} - {}^2E_{1/2,\ \text{ETDI-TBA}}$), respectively. This is well correlated with the LUMO level stabilization of ETTI observed in the DFT calculation (*vide supra*).

Since the concentration and the type of electrolyte cation can affect the redox potential,[42-43] we measured CV of the imides with 2 M lithium bis(trifluoromethanesulfonyl)imide (LiTFSI) in tetraethylene glycol dimethyl ether (TEGDME), which is the same electrolyte used in the Li-ion coin cell test (*vide infra*). The measured reduction potentials are -0.99 V (${}^1E_{1/2,\ \text{ETDI-Li}}$) and -1.22 V (${}^2E_{1/2,\ \text{ETDI-Li}}$) vs. Ag/Ag$^+$ for ETDI and -0.60 V (${}^1E_{1/2,\ \text{ETTI-Li}}$), -0.86 V (${}^2E_{1/2,\ \text{ETTI-Li}}$), and -1.42 V (${}^3E_{1/2,\ \text{ETTI-Li}}$) vs. Ag/Ag$^+$ for ETTI, respectively. According to Nernst equation, the concentration increase of the electrolyte should lead to a drop in the redox potential.[43] However, both ETDI and ETTI show increased reduction potentials in the 2 M of Li-containing electrolyte compared to those in the 0.1 M of TBA salt-based electrolyte (see Figure 2c, d). This is most likely attributed to that the smaller Li cation has a greater electrostatic interaction with a reduced imide molecule and thereby form a more stable ion complex than the TBA$^+$ ion.

Furthermore, it is worth noticing that the first and second reduction potentials of ETTI are considerably more elevated than ETDI in the Li$^+$ based electrolyte (Table S1, S2 in SI). The potential differences of ETTI in between the Li$^+$ and TBA$^+$ based electrolytes are 0.37 (${}^1E_{1/2,\ \text{ETTI-Li}} - {}^1E_{1/2,\ \text{ETTI-TBA}}$) and 0.76 V (${}^2E_{1/2,\ \text{ETTI-Li}} - {}^2E_{1/2,\ \text{ETTI-TBA}}$) for the first and second reduction, while those of ETDI are 0.17 (${}^1E_{1/2,\ \text{ETDI-Li}} - {}^1E_{1/2,\ \text{ETDI-TBA}}$) and 0.54 V (${}^2E_{1/2,\ \text{ETDI-Li}} - {}^2E_{1/2,\ \text{ETDI-TBA}}$), respectively. As a result, in the Li$^+$ based electrolyte, the first and second reduction potentials of ETTI turn out to be much higher than those of ETDI by 0.39 V (${}^1E_{1/2,\ \text{ETTI-Li}} - {}^1E_{1/2,\ \text{ETDI-Li}}$) and 0.36 V (${}^2E_{1/2,\ \text{ETTI-Li}} - {}^2E_{1/2,}$

$_{\text{ETDI-Li}}$), respectively. We hypothesized that such an additional elevation of reduction potentials of ETTI would be attributable to certain additional interactions between adjacent two carbonyl groups in ETTI and the inserted Li^+ ion during the reduction.[16]

Computational calculation

To shed light on the additional potential elevation of ETTI, we conducted computational calculations on the theoretical reduction potentials of the imides with various counter cations using the DFT method (The detailed calculation process is fully described in SI). ETTI and ETDI show a different number of reduction reactions, but the reactions occur in a stepwise fashion. For the comparative study, we therefore focused on investigating the energetics of the first reduction reaction to form anions of the imide molecules in the calculation. The calculated Gibbs free energies of the molecules are summarized in Table S3-6.

First, we examined the reduction process of the two imides without involving a counter cation. In the neutral state, both ETTI and ETDI have planar geometries (Figure S12 and S13 in SI). Upon reduction by an electron, the two imides show no significant changes in their geometries. The theoretical reduction potentials are calculated to be 2.25 and 2.02 V *vs.* Li/Li^+ for ETTI and ETDI, respectively. ETTI showed 0.23 V higher theoretical reduction potential than ETDI consistent with the LUMO level shift due to the electron-withdrawing effect of the additional imide group.

Next, we considered the insertion of a counter cation for charge compensation and the interactions between the counter cation and the anion of the imides. To reduce calculation cost, we used a tetramethylammonium (TMA) cation bearing the shortest alkyl chains instead of a TBA^+ ion bearing long butyl chains. In the case of ETDI, upon reduction, the inserted TMA^+ ion is located in the close vicinity of a carbonyl oxygen atom of an imide group without distortion of the molecular backbone (Figure S14a). On the other hand, due to a smaller ion radius, the Li^+ ion is more closely located to the carbonyl oxygen and thereby forms a coordinate bond ($r_{\text{O-Li}}$ = 1.78 Å), resulting in a more stable ion complex with ETDI than the TMA^+ ion (Figure 2e and S15a). The calculated reduction potentials of ETDI are 2.22 and 2.99 V vs. Li/Li^+ for the TMA^+ and Li^+ ion insertion, respectively. Based on the above results, we attribute the increased reduction potentials of ETDI with

Li-ion than TBA^+ ion in the CV studies to the formation of a more stable ion complex (*vide supra*).

Interestingly, in the case of ETTI, we found that the inserted counter cation can interact with two carbonyl oxygen atoms of the two different imide groups. As shown in Figure S14b, the inserted TMA-ion is in close proximity to both two carbonyl oxygen atoms by reduction, but its bulky alkyl groups hinder their direct contact. In sharp contrast, the small Li^+ ion can be positioned between the two carbonyl oxygen atoms and thereby be bound by coordination bonds ($r_{\mathrm{o1\text{-}Li}}$ = 1.87 Å and $r_{\mathrm{o2\text{-}Li}}$ = 1.87 Å) to form a 7-membered ring without significant geometrical distortion of the molecular backbone (Figure 2f and S15b). Such unique Li-O interactions considerably stabilize the energy of the ETTI-Li complex, leading to further elevation of the reduction potential of ETTI in the Li^+ based electrolyte. The calculated theoretical reduction potentials of ETTI are 2.53 and 3.70 V vs. Li/Li^+ for TMA^+ and Li^+ ion insertion, respectively.

To get more insight into the cation coordination effect on the reduction potential, we performed DFT calculations on a sodiated and a potassiated ETTI. The DFT calculation revealed that a sodium and a potassium cation is also bound to two carbonyl oxygen atoms of different imide groups of ETTI to form a 7-membered ring without distortion by reduction (Figure S16), like the Li cation case. But, the length of coordination bond between the cation and the oxygen atom ($r_{O\text{-}cation}$) gradually increases as the ionic radius gets larger ($r_{O\text{-}Li}$ = 1.87 Å, $r_{O\text{-}Na}$ = 2.23 Å, and $r_{O\text{-}K}$ = 2.58 Å). Correspondingly, the calculated first reduction potential of ETTI decreases to 3.34 V and 3.24 V vs. Li/Li+ for the Na^+ and K^+ case, respectively. Therefore, it is expected that the reduction potentials of ETTI can be tuned by varying counter ions.

The calculated values of the reduction potentials have difference from the actual values in the CV experiments, particularly in the case of Li-based electrolyte, which is most likely due to overestimation of the stabilization energy of Li-O coordination bond in the DFT calculation. Nevertheless, it should be noted that the DFT calculation results well explain the potential shift trend of the imide materials in the electrolytes containing different cations, which is observed in the CV measurements shown above.

Li-ion cell test

Encouraged by the reversible redox reactions with three electrons and the elevated redox potentials of ETTI in the solution CV, we tested ETTI as a cathode material in Li-ion coin cells. First, we checked the performance of ETTI electrode using Super P as a conductive material (ETTI : SuperP : PVDF = 4 : 4 : 2, w/w/w) in the two different commonly used electrolytes: one was 1 M $LiPF_6$ in a 3:7 (v/v) mixture of ethylene carbonate (EC) and dimethyl carbonate (DMC), and the other was 1 M lithium bis(trifluoromethanesulfonyl) imide (LiTFSI) in TEGDME. At the initial cycle, a higher specific capacity was delivered in the ether-based TEGDME electrolyte (78 mAh g^{-1}) than in the carbonate-based electrolyte (EC/DMC) (33 mAh g^{-1}, see Figure S4), which is most likely due to lower solubility of ETTI in the ether-based solvents.

Next, to suppress dissolution of ETTI, the concentration of LiTFSI salt was increased to 2 M because high concentration electrolyte can effectively retard the dissolution of active material due to common ion effect.[18, 44] Indeed, the ETTI electrode delivered a higher specific capacity in 2 M LiTFSI electrolyte (105 mAh g^{-1}) than in 1 M (78 mAh g^{-1}) at the first cycle and retained higher specific capacities at the subsequent cycles (Figure S3).

Then, we changed the solvent of the electrolyte from TEGDME to a 1:1 (v/v) mixture of 1,3-dioxolane (DOL) and dimethoxyethane (DME). However, the ETTI electrode delivered much lower specific capacity (80 mAh g^{-1}) in this electrolyte (see Figure S4). Therefore, we chose 2 M LiTFSI in TEGDME as an electrolyte for further study. But, even after the electrolyte optimization process, the ETTI electrode still delivered a low specific capacity compared to its theoretical maximum. One of the reasons for the low capacity utilization is probably due to the low electrical conductivity of the organic active material. Therefore, we introduced graphene as a conductive material instead of Super P to compensate the poor electrical conductivity of the active material.

Finally, we fabricated electrodes containing either ETTI or ETDI as an active material with graphene as a conductive additive and polyvinylidene fluoride (PVDF) as a binder in a weight ratio of 4:4:2 and subtracted the specific capacity of the graphene itself from those of all electrodes, respectively. In a Li-ion coin cell with 2 M LiTFSI in TEGDME electrolyte, ETTI electrode recorded a specific capacity of 220 mAh g^{-1} ($C_{ETTI,\ discharge}$) at the initial cycle; but it included a specific capacity from graphene ($C_{graphene}$ = 44 mAh g^{-1}) (see Figure S5 and S6). After removing specific capacity from the graphene, ETTI delivered a specific capacity of 176 mAh g^{-1} ($C_{ETTI,\ discharge}$ - $C_{graphene}$) from only active material at the first cycle, which corresponds to 81% of its theoretical capacity. In addition, as can be seen in Figure 3a, the voltage *vs.* capacity profile of ETTI clearly shows three voltage plateaus.

These unambiguously indicate redox reactions with three electrons. In its differential capacity (dQ/dV) plot (Figure 3b), the discharge/recharge peaks of the ETTI electrode are observed at 2.82/2.92, 2.31/2.58, and 2.09/2.14 V vs. Li/Li$^+$, respectively, coinciding with the CV results.

In contrast, the ETDI electrode shows a specific capacity of 63 mAh g^{-1} from the active material ($C_{ETDI, discharge}$ - $C_{graphene}$) at the first cycle with a slopy voltage profile (Figure 3a and S6). Such low capacity utilization (32% of its theoretical capacity) of ETDI is likely due to the prompt dissolution of the active materials into the electrolyte solution. Nevertheless, in the dQ/dV plot, two discharge/recharge peaks are observed, which are 2.22/2.33 and 2.13/2.11 V vs. Li/Li$^+$, respectively (Figure 3b). It should be noted that not only the first and second reduction potentials of ETTI but also its average discharge voltage is elevated than ETDI in the Li-ion cells ($V_{discharge,avg}$ = 2.41 and 2.18 V vs. Li/Li$^+$ for ETTI and ETDI, respectively). Most importantly, the elevated average discharge voltage (2.41 V) with the high specific capacity (176 mAh g^{-1}) of ETTI led to its high specific energy up to 421 Wh kg^{-1}, which is even higher than the non-substituted PDI (301 Wh kg^{-1}) and PyDI (385 Wh kg^{-1}) reported previously (Figure 3d). Theoretically, the specific energy of ETTI can be achieved as high as 523 Wh kg^{-1}, exceeding that of other DI-based electrode materials. Furthermore, considering the high theoretical specific capacity of unsubstituted MTI building block (282 mAh g^{-1}), it has the potential to draw a specific energy up to 680 Wh kg^{-1}.

Although ETTI shows improved specific capacity and discharge voltage than ETDI, its specific capacity rapidly decayed during the subsequent charge/discharge cycles due to its high solubility in the electrolyte solution.[7] The dissolution of the ETTI electrode into the electrolyte was confirmed by UV-vis absorption spectroscopy. When the pristine ETTI electrode was soaked in the electrolyte, absorbance of the solution gradually increased as time passed, indicating dissolution of the ETTI molecules into the electrolyte (Figure S8). In addition, after 10 cycles of charge/discharge, we found that the separator of the cell was colored. This is most likely due to that the reduced ETTI molecules dissolved into the electrolyte and then penetrated into the separator during the charge/discharge cycles (Figure S9). To overcome this solubility problem, we synthesized BZTI (see Figure 1 for its molecular structure and synthesis scheme) by introducing heavier substituents such as benzyl groups instead of the ethyl groups at the N-positions because organic materials possessing higher molecular weight typically show lower solubility in organic solvents. The galvanostatic measurement of BZTI electrode shows the initial specific capacity of 127 mAh g^{-1} from only active material ($C_{BZDI, discharge}$ - $C_{graphene}$), corresponding 88% of the theoretical capacity ($C_{theo.BZTI}$ = 145 mAh g^{-1}) with average discharge voltage of 2.38 V vs. Li/Li^+ (Figure 3a and S6). As expected, the BZTI electrode exhibits much improved cycle retention after 20 cycles (Figure 3c and S7).

Charge/Discharge Mechanism

To elucidate the redox mechanism of MTI in the Li-ion cell, fully discharged and recharged ETTI electrodes were analyzed through ex-situ Fourier-transform infrared (FT-IR) spectroscopy. In the pristine electrode, two carbonyl (C=O) peaks of imide groups appear at 1720 and 1773 cm^{-1}, corresponding to asymmetric and symmetric stretching vibrations, respectively. Upon discharge to 1.7 V, these carbonyl peaks are attenuated while new strong and broad peaks appear at 1590-1630 cm^{-1}, which can be assigned to C-O-Li of the reduced ETTI (Figure 4a).[28, 37, 45] And then, after recharge to 3.5 V, the broad Li-enolate peaks disappear, and the original carbonyl peaks are restored, indicating reversible charge/discharge of ETTI. In addition, the ex-situ FT-IR measurements of the BZTI electrode during charge/discharge also indicates that its redox mechanism is identical to that of the ETTI electrode (Figure S10).

We further investigated the redox mechanism of ETTI using DFT calculation, and the calculated lithiation pathway of ETTI is shown in Figure 4b. First, when a Li-ion is inserted into a reduced ETTI molecule with one electron, the Li-ion binds with the adjacent two carbonyl oxygen atoms of the two different imide groups to form Li-ETTI. The second and third Li-ion is inserted into a similar position and also binds with two carbonyl oxygen atoms of the rest imide groups to form Li_2-ETTI and Li_3-ETTI, respectively, in a stepwise fashion. Finally, we simulated the FT-IR spectra of ETTI and Li_3-ETTI, and the predicted spectra well coincide with the ex-situ FT-IR measurements (see Figure S11).

Conclusion

In summary, we report a novel C3 symmetric MTI as a new building block for electrode materials with high specific capacity and energy. A model compound ETTI undergoes three reversible redox reactions at -0.97 V, -1.62 V, and -2.34 V vs. Ag/Ag^+, respectively, with 0.1 M TBAHFP electrolyte in the solution CV measurement. But, ETTI showed much elevated redox potentials with 2 M LiTFSI electrolyte, which are -0.60 V, -0.86 V, and -1.42 V vs. Ag/Ag$^+$ for ETTI, respectively. The DFT calculation revealed that the potential elevation of ETTI is attributed not only to the mutual electron-withdrawing effect of three imide groups but also to the formation of the stable coordination bonds between the adjacent two imide groups and an inserted Li$^+$ ion. In a Li ion coin cell, compared to the PyDI-based model compound ETDI, ETTI delivered much improved specific capacity (176 mAh g^{-1}) with three electrons and showed elevated average discharge voltage (2.41 V), allowing ETTI to deliver one of the highest specific energy (421 Wh kg^{-1}) among reported DI-based electrode materials. Finally, the redox mechanism of ETTI in the Li-coin cell was investigated by ex-situ FT-IR and DFT calculation.

Through this study, we found that adding a more redox center at an appropriate position in a DI molecule can effectively increase both the redox potential and specific capacity. Considering the theoretical maximum capacity (282 mAh g^{-1}), the new building block MTI proposed in this study has potential to deliver high specific energy up to 680 Wh kg^{-1}, exceeding that of conventional transition metal oxide cathodes such as $LiCoO_2$ (546 Wh kg^{-1}) or $LiFePO_4$ (578 Wh kg^{-1}).[46] However, further engineering of MTI-based active materials is needed to achieve high cycle stability with full utilization of specific capacity, such as preparing MTI-based polymers or using ionic liquids as an electrolyte. In addition, it can be expected that introducing our molecular design strategy of multi-imide into NDI- and PDI-based electrode materials, which possess a more extended π-conjugated core than PyDI and MTI, would lead to higher average discharge voltage above 2.5 V *vs.* Li/Li$^+$. We believe that our material design can provide a breakthrough to improve the electrochemical performance of the organic electrode.

Experimental Section

Materials and General Methods: Chemicals were purchased from commercial suppliers and used without further purification unless otherwise stated. Lithium bis(trifluoromethanesulfonyl)imide (LiTFSI) and tetraethylene glycol dimethyl ether (TEGDME) were purchased from Sigma-Aldrich, and mellitic acid was purchased from TCI. Reactions were monitored using thin-layer chromatography (TLC) with commercial TLC plates (silica gel 60 F254, Merck Co.). Silica gel column chromatography was performed with silica gel 60 (particle size 0.063-0.200 mm, Merck Co.). ^{1}H-NMR and ^{13}C-NMR spectra were recorded on a Bruker Avance 300 spectrometer. Mass spectra were measured using a JEOL, JMS-700 mass spectrometer. ATR/FT-IR was performed on a Thermoscientific Nicolet 6700 spectrometer.

Synthesis of ETTI: To an aqueous solution of mellitic acid (2g, 5.85mmol) in a round bottom flask (500 mL) was added a solution of ethylamine (0.79 g, 17.55 mmol, 69 wt% in water) with stirring. After 0.5 h sonication, the water was evaporated by a vacuum pump. The solid was then heated to 140 °C in an oven for 4 days. After cooling down to room temperature, to the solid, chloroform and silica gel were added with sonication. After evaporating the solvents, the remnant solid was added to silica gel column and purified by chromatography using 1:1 (v/v) ethylacetate/n-hexane eluent mixture to afford ETTI (Yield = 32%, white powder). ^{1}H NMR (300 MHz, CDCl3, δ): 3.88 (q, 6H), 1.33 (t, 9H); ^{13}C NMR (125 MHz, CDCl3, δ): 162.5, 133.6, 34.5, 13.7; MS (FAB+) m/z: calcd. for $C_{18}H_{15}N_3O_6$ 369.10, found 370.10 (M+1).

Synthesis of BZTI: To an aqueous solution of mellitic acid (2g, 5.85mmol) in a round bottom flask (500mL) was added a solution of benzylamine (1.88g, 17.55 mmol) with stirring. After 0.5 h sonication, the water was evaporated by a vacuum pump. The solid was then heated to 140 °C in an oven for 4 days. After cooling down to room temperature, to the solid, chloroform and silica gel were added with sonication. After evaporating the solvents, the remnant solid was added to silica gel column and purified by chromatography using 25:1 (v/v) dichloromethane/ethylacetate eluent mixture (Yield = 14%, white powder). ^{1}H NMR (300 MHz, CDCl3, δ): 7.47 (m, 6H), 7.29-7.27 (m, 9H), 4.93 (s, 6H); ^{13}C NMR (125 MHz, CDCl3, δ): 162.23, 135.07, 133.68, 129.58, 129.05, 128.64, 43.08; MS (FAB+) m/z: calcd. for $C_{33}H_{21}N_3O_6$ 555.14, found 556.15 (M+1)

Synthesis of ETDI: The anhydrous pyromellitic acid (1g, 4.58mmol) was dissolved in 15 mL of dimethylformamide (DMF), and then to the solution, ethyl amine (0.49g, 10.87mmol) was added dropwise. The mixture was refluxed at 150 °C. After monitoring the reaction was finished by TLC, the solution was cooled down to room temperature, and the organic layer was extracted three times with water and dichloromethane. The product dried by $MgSO_4$ was purified by silica gel column chromatography using 1:6 (v/v) ethylacetate/n-hexane eluent mixture (Yield = 12%, pale yellow powder). ^1H NMR (300 MHz, CDCl3, δ): 8.27 (s, 2H), 3.84-3.77 (q, 4H), 1.34-1.29 (t, 6H); ^{13}C NMR (125 MHz, CDCl3, δ): 166.31, 137.52, 118.29, 33.85, 14.01; MS (FAB+) m/z: calcd. for $C_{14}H_{12}N_2O_4$ 272.08, found 273.08 (M+1)

Electrochemical Measurement: Cyclic voltammetry (CV) was performed on a Princeton Applied Research Model 273a using a three-electrode beaker cell with an Ag wire in 0.01 M $AgNO_3$ solution as a reference electrode, a glassy carbon disc (diameter = 3 mm) as a working electrode, and a platinum wire as a counter electrode, respectively. The redox potential of the reference electrode was calibrated using ferrocene/ferrocenium (Fc/Fc^+) as an internal standard. The concentration of ETTI and ETDI solutions for the CV measurements with 0.1 M TBAHFP as the supporting electrolyte was 5×10^{-3} M in CH_3CN but was 1×10^{-3} M for BZTI due to its low solubility. To measure the solution CV with 2M LiTFSI as the supporting electrolyte, the solution of ETTI and ETDI (1×10^{-3} M in TEGDME) was prepared and measured in a glove box to prevent exposure to air.

Cathode Fabrication and Galvanostatic Test: Slurries of the active materials (ETTI, BZTI, and ETDI), graphene (graphene nanoplatelets, surface area 750 m^2 g^{-1}, Sigma Aldrich), and polyvinylidene fluoride (PVDF, Kureha KF L#7208) in N-methyl-2-pyrrolidone (NMP, 99%, TCI) were prepared with a weight ratio of 4:4:2. The slurries were stirred overnight at room temperature and then spread on aluminum foils by doctor blading. The electrodes were dried at 120 °C for 8 h in a vacuum oven and punched into circular discs to a diameter of 14 mm. Coin type CR2032 (Hohsen) cells were assembled with the fabricated cathodes, a Li-metal anode, and a polypropylene separator (Celgard 2400) in an Ar-filled glove box (Korea Kiyon KK-011-AS) in which moisture and oxygen levels were tightly regulated under 0.5 ppm. The galvanostatic discharge/charge tests of the coin cells were performed on a battery cycler (Wonatech WBCS3000L) at 30 °C.

Ex-situ FT-IR Measurement for Redox Mechanism Study: Different states of electrodes, which are as-prepared, discharged to 1.7 V, and recharged to 3.5 V, were prepared, respectively for ex-situ FT-IR measurements. To prevent exposure to air, all samples were moved to Ar-filled glove box before opening the coin cells. After disassembling the coin cells, the electrodes were washed several times with 1,4-dioxolane (DOL) and dimethoxyethane (DME) to remove the residual electrolytes. Subsequently, the residual solvents were removed from the electrode in a vacuum chamber. Then, the electrodes were sealed in Ar-filled vials. FT-IR measurements were conducted with Thermoscientific Nicolet 6700 spectrometer. The spectra were recorded using ATR accessory in 600-4000 cm^{-1} wavenumber.

Acknowledgment

This work was supported in parts by the Presidential Post-doc Fellowship Program through the National Research Foundation of Korea (NRF) funded by the Ministry of Education (2016R1A6A3A04008134[RIAM0417-20180002]) , the National R&D Program through the National Research Foundation of Korea (NRF) funded by the Ministry of Science & ICT (No. 2017M3A7B4041699), and the project by Samsung Advanced Institute of Techonology (0417-20190113)

Thanks to Sechan Lee and Giyun Kwon in professor Kisuk Kang group for their advice and assistance in measuring CV with Li-based electrolyte in the glove box.

Scheme 1

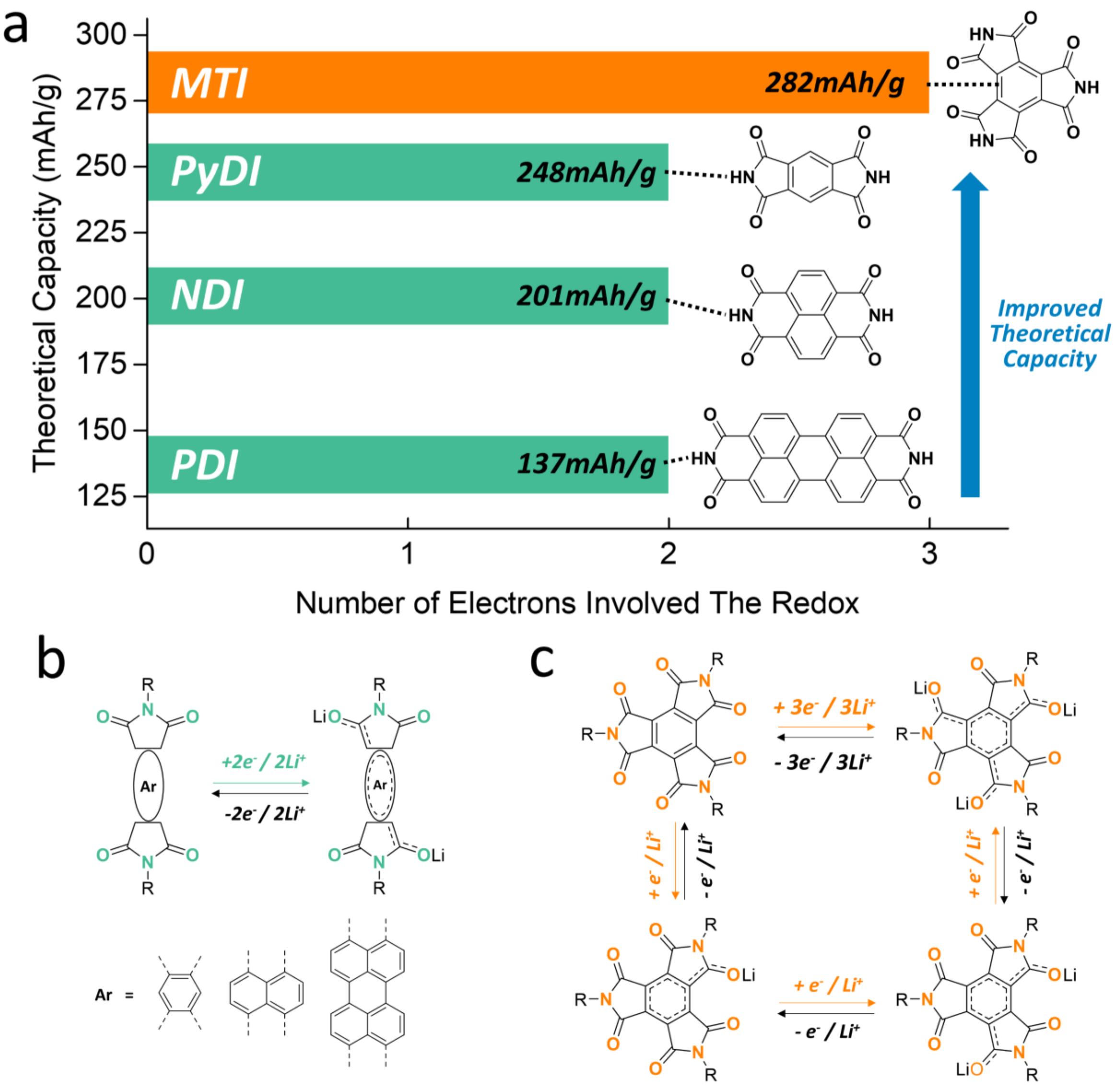

Scheme1. (a) The maximum theoretical specific capacity and the number of electrons participated in the redox reactions of the DI building blocks. The redox reaction schemes of (b) PyDIs, NDIs, PDIs, (c) and MTIs.

Figure 1

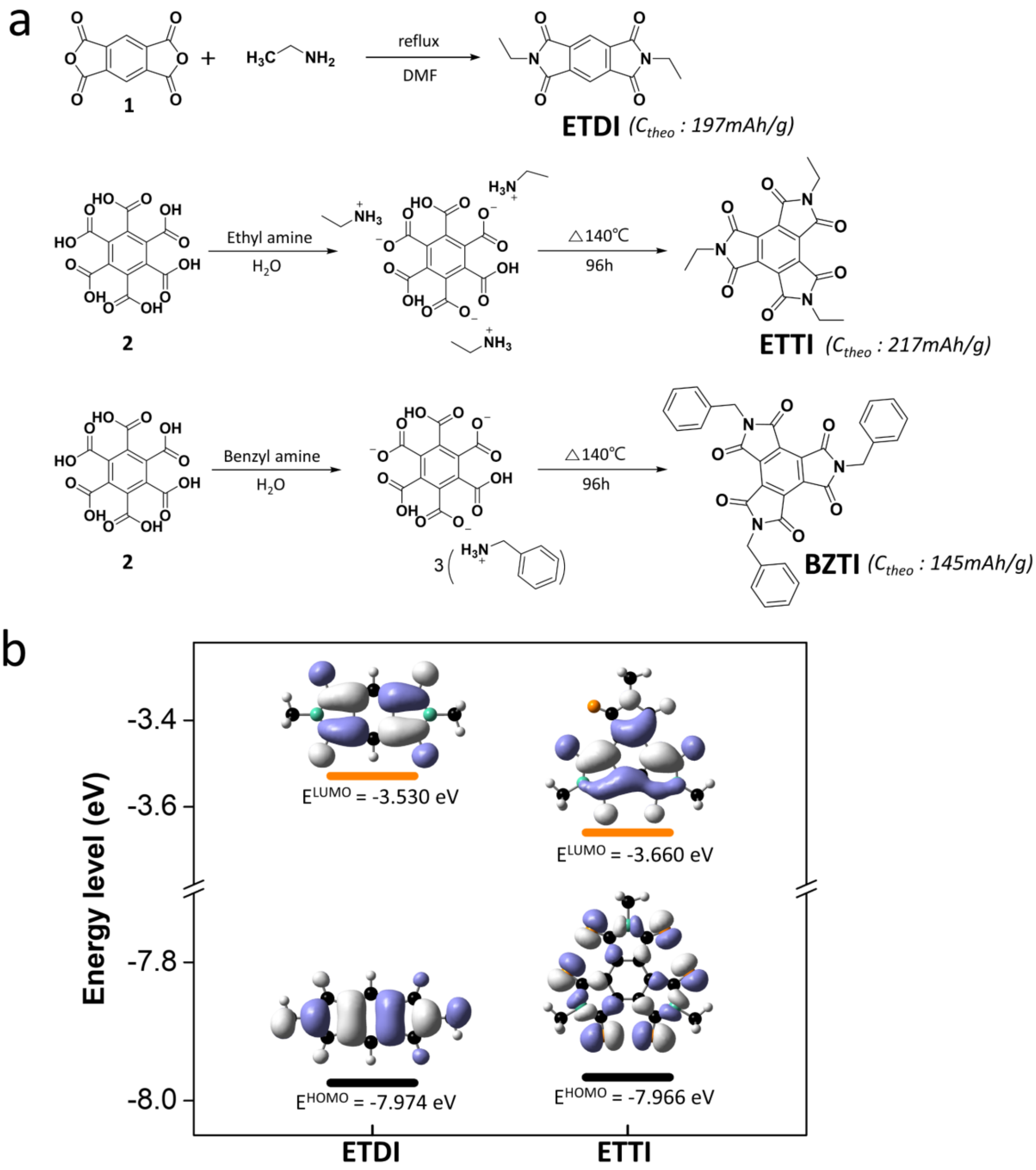

Figure 1. (a) Synthesis schemes of ETDI, ETTI, and BZTI. (b) HOMO/LUMO levels and the corresponding orbital diagrams of ETDI and ETTI.

10.1002/cssc.202000180

Figure 2

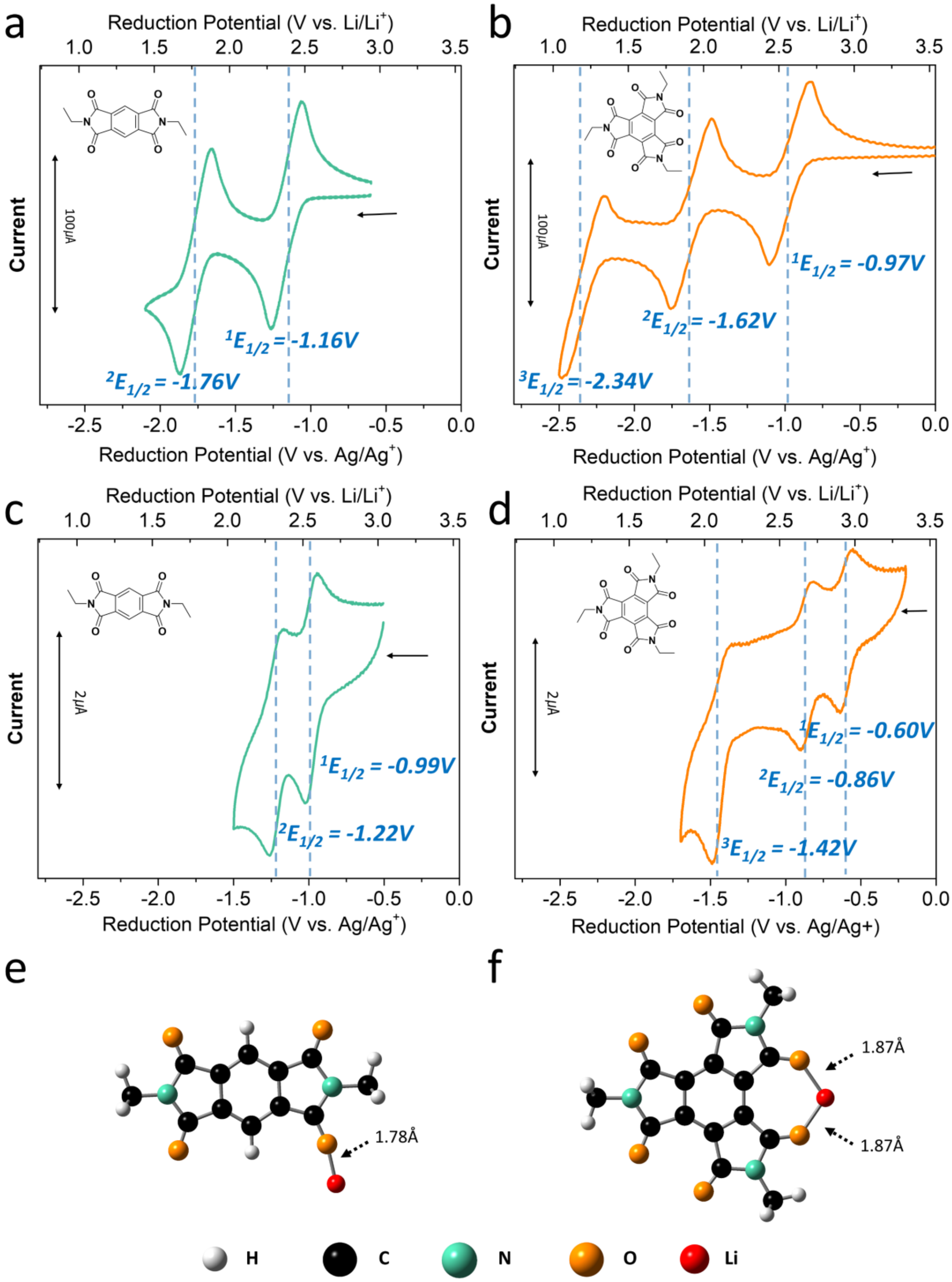

Figure 2. CV data of (a) ETDI and (b) ETTI in 0.1 M TBAHFP acetonitrile solution. CV data of (c) ETDI and (d) ETTI in 2 M LiTFSI in TEGDME solution. Scan rate (*v*) was 50 mV s^{-1} and the concentrations of ETDI and ETTI were 5 × 10^{-3} M for acetonitrile solutions and 1 × 10^{-3} M for TEGDME solutions. The optimized geometries of (e) Li-ETDI and (f) Li-ETTI from DFT calculation.

10.1002/cssc.202000180

Figure 3

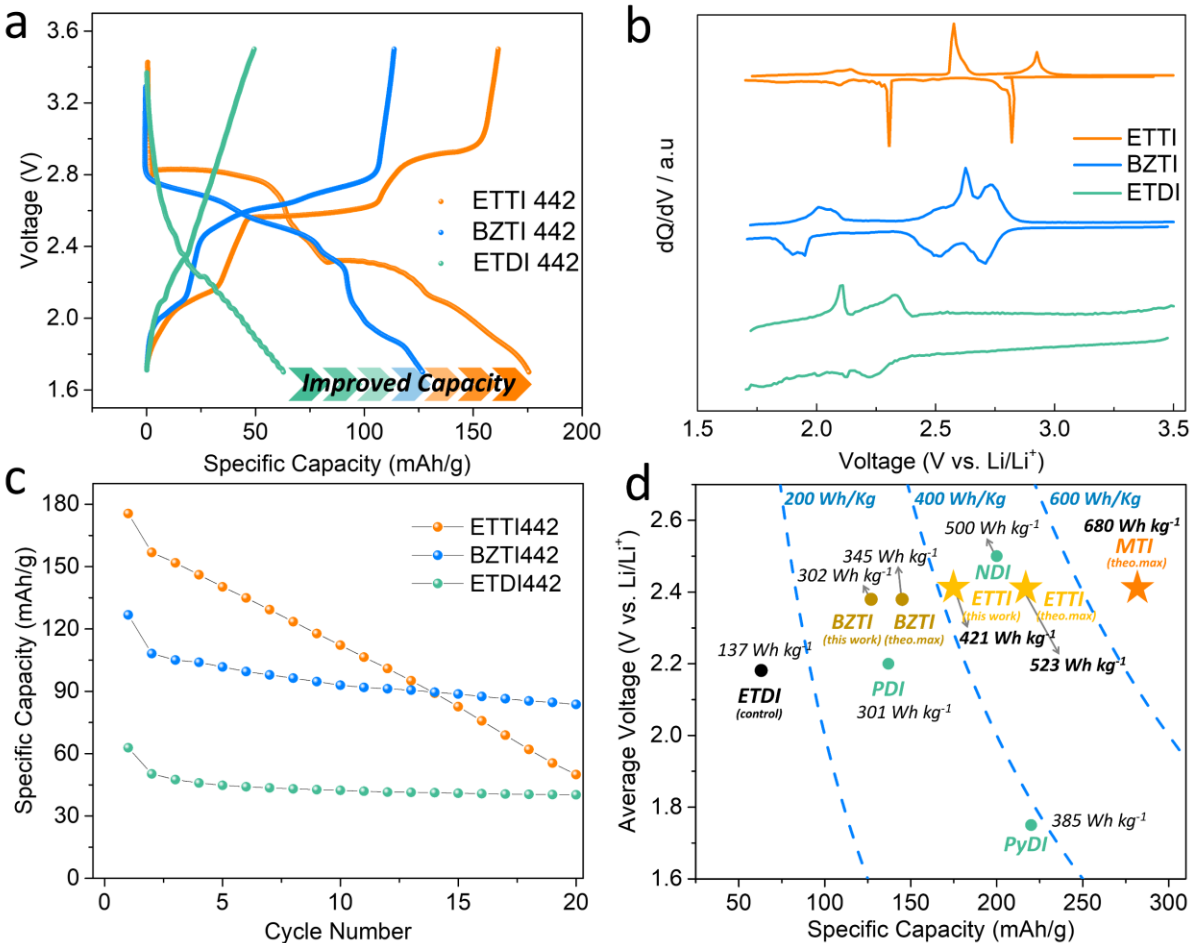

Figure 3. The initial voltage vs specific capacity profiles of (a) ETTI, BZTI, and ETDI electrodes at 0.1C rate. (b) The representative dQ/dV plot of ETTI, BZTI, and ETDI. (c) The cycling test of ETTI, BZTI, and ETDI at 0.1C rate. (d) The plot of average voltage vs. specific capacity with the specific energy regarding MTIs and DIs. The previously reported highest energy densities using PyDI,[36] NDI,[37] and PDI[47] are presented as green circles.

Figure 4

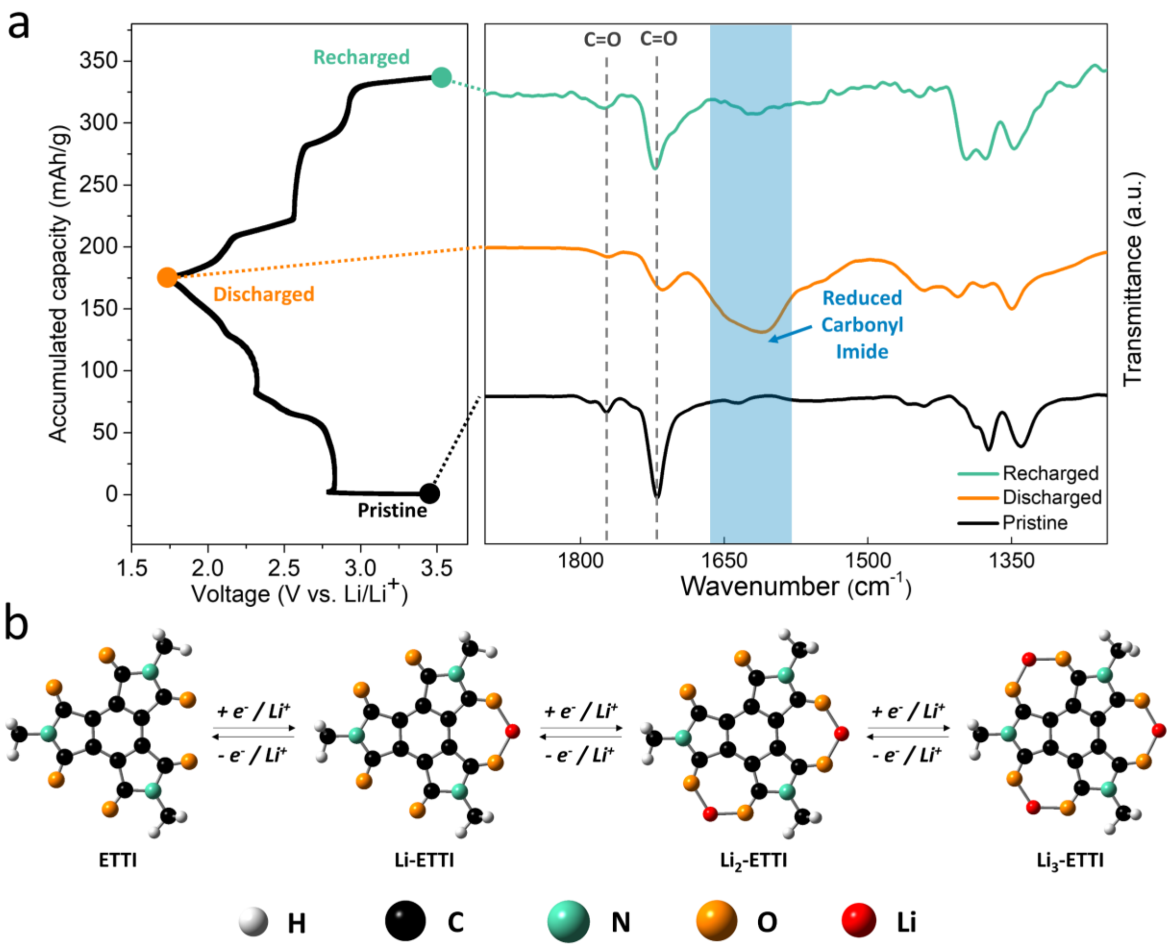

Figure 4. (a) Ex situ FT-IR spectra (right panel) of the ETTI electrode with the accumulated capacity vs voltage profile (left panel) at the state of pristine, discharged, and charged. (b) The optimized geometries of ETTI, Li-ETTI, Li_2-ETTI and Li_3-ETTI from DFT calculation.

[1] J. M. Tarascon, M. Armand, *Nature* **2001**, *414*, 359-367.

[2] J. B. Goodenough, K. S. Park, *J. Am. Chem. Soc.* **2013**, *135*, 1167-1176.

[3] M. Armand, J. M. Tarascon, *Nature* **2008**, *451*, 652-657.

[4] J. Xie, Q. Zhang, *Small* **2019**, *15*, e1805061.

[5] X. Zeng, M. Li, D. Abd El-Hady, W. Alshitari, A. S. Al-Bogami, J. Lu, K. Amine, *Adv. Energy Mater.* **2019**, *9*, 1900161.

[6] Y. Lu, Q. Zhang, L. Li, Z. Niu, J. Chen, *Chem* **2018**, *4*, 2786-2813.

[7] S. Muench, A. Wild, C. Friebe, B. Haupler, T. Janoschka, U. S. Schubert, *Chem. Rev.* **2016**, *116*, 9438-9484.

[8] Y. Liang, Z. Tao, J. Chen, *Adv. Energy Mater.* **2012**, *2*, 742-769.

[9] W. Choi, S. Ohtani, K. Oyaizu, H. Nishide, K. E. Geckeler, *Adv. Mater.* **2011**, *23*, 4440-4443.

[10] O. Kenichi, N. Hiroyuki, *Adv. Mater.* **2009**, *21*, 2339-2344.

[11] N. Oyama, T. Tatsuma, T. Sato, T. Sotomura, *Nature* **1995**, *373*, 598-600.

[12] S. R. Deng, L. B. Kong, G. Q. Hu, T. Wu, D. Li, Y. H. Zhou, Z. Y. Li, *Electrochim. Acta* **2006**, *51*, 2589-2593.

[13] D. J. Min, F. Miomandre, P. Audebert, J. E. Kwon, S. Y. Park, *ChemSusChem* **2019**, *12*, 503-510.

[14] M. Armand, S. Grugeon, H. Vezin, S. Laruelle, P. Ribiere, P. Poizot, J. M. Tarascon, *Nat Mater* **2009**, *8*, 120-125.

[15] L. Fédèle, F. Sauvage, S. Gottis, C. Davoisne, E. Salager, J.-N. Chotard, M. Becuwe, *Chem. Mater.* **2017**, *29*, 546-554.

[16] S. Lee, J. E. Kwon, J. Hong, S. Y. Park, K. Kang, *J. Mater. Chem. A* **2019**, *7*, 11438-11443.

[17] J. Lee, M. J. Park, *Adv. Energy Mater.* **2017**, *7*, 1602279.

[18] K. Zhang, C. Guo, Q. Zhao, Z. Niu, J. Chen, *Adv. Sci.* **2015**, *2*, 1500018.

[19] Y. Liang, P. Zhang, J. Chen, *Chem. Sci.* **2013**, *4*, 1330-1337.

[20] H. Banda, D. Damien, K. Nagarajan, A. Raj, M. Hariharan, M. M. Shaijumon, *Adv. Energy Mater.* **2017**, *7*, 1701316.

[21] N. Zindy, J. T. Blaskovits, C. Beaumont, J. Michaud-Valcourt, H. Saneifar, P. A. Johnson, D. Bélanger, M. Leclerc, *Chem. Mater.* **2018**, *30*, 6821-6830.

[22] G. Wang, N. Chandrasekhar, B. P. Biswal, D. Becker, S. Paasch, E. Brunner, M. Addicoat, M. Yu, R. Berger, X. Feng, *Adv. Mater.* **2019**, *31*, 1901478.

[23] Y. Liang, Z. Chen, Y. Jing, Y. Rong, A. Facchetti, Y. Yao, *J. Am. Chem. Soc.* **2015**, *137*, 4956-4959.

[24] A. E. Lakraychi, K. Fahsi, L. Aymard, P. Poizot, F. Dolhem, J. P. Bonnet, *Electrochem. Commun.* **2017**, *76*, 47-50.

[25] D. J. Kim, K. R. Hermann, A. Prokofjevs, M. T. Otley, C. Pezzato, M. Owczarek, J. F. Stoddart, *J Am Chem Soc* **2017**, *139*, 6635-6643.

[26] H.-g. Wang, S. Yuan, D.-l. Ma, X.-l. Huang, F.-l. Meng, X.-b. Zhang, *Adv. Energy Mater.* **2014**, *4*.

[27] B. Tian, J. Zheng, C. Zhao, C. Liu, C. Su, W. Tang, X. Li, G.-H. Ning, *J. Mater. Chem. A* **2019**, *7*, 9997-10003.

[28] T. Bančič, J. Bitenc, K. Pirnat, A. Kopač Lautar, J. Grdadolnik, A. Randon Vitanova, R. Dominko, *J. Power Sources* **2018**, *395*, 25-30.

[29] S. Gheytani, Y. Liang, F. Wu, Y. Jing, H. Dong, K. K. Rao, X. Chi, F. Fang, Y. Yao, *Adv. Sci.* **2017**, *4*, 1700465.

[30] A. Ahmad, H. Wu, Y. Guo, Q. Meng, Y. Meng, K. Lu, L. Liu, Z. Wei, *RSC Adv.* **2016**, *6*, 33287-33294.

[31] Z. Song, H. Zhou, *Energy Environ. Sci.* **2013**, *6*, 2280-2301.

[32] B. Häupler, A. Wild, U. S. Schubert, *Adv. Energy Mater.* **2015**, *5*, 1402034.

[33] S. Renault, V. A. Mihali, K. Edström, D. Brandell, *Electrochemistry Communications* **2014**, *45*, 52-55.

[34] D. Chen, A. J. Avestro, Z. Chen, J. Sun, S. Wang, M. Xiao, Z. Erno, M. M. Algaradah, M. S. Nassar, K. Amine, Y. Meng, F. S. J, *Advanced Materials* **2015**, *27*, 2907-2912.

[35] T. B. Schon, A. J. Tilley, E. L. Kynaston, D. S. Seferos, *ACS Applied Materials & Interfaces* **2017**, *9*, 15631-15637.

[36] S. Renault, J. Geng, F. Dolhem, P. Poizot, *Chem. Commun.* **2011**, *47*, 2414-2416.

[37] Y. Shi, H. Tang, S. Jiang, L. V. Kayser, M. Li, F. Liu, F. Ji, D. J. Lipomi, S. P. Ong, Z. Chen, *Chem. Mater.* **2018**, *30*, 3508-3517.

[38] H. Kim, J. E. Kwon, B. Lee, J. Hong, M. Lee, S. Y. Park, K. Kang, *Chem. Mater.* **2015**, *27*, 7258-7264.

[39] G. S. Vadehra, R. P. Maloney, M. A. Garcia-Garibay, B. Dunn, *Chem. Mater.* **2014**, *26*, 7151-7157.

[40] K. A. McMenimen, D. G. Hamilton, *J. Am. Chem. Soc.* **2001**, *123*, 6453-6454.

[41] K. G. Rose, D. A. Jaber, C. A. Gondo, D. G. Hamilton, *J. Org. Chem.* **2008**, *73*, 3950-3953.

[42] M. Lee, J. Hong, B. Lee, K. Ku, S. Lee, C. B. Park, K. Kang, *Green Chem.* **2017**, *19*, 2980-2985.

[43] A. J. Bard, L. R. Faulkner, *Electrochemical Methods: Fundamentals and Applications*, Wiley, **2000**.

[44] E. S. Shin, K. Kim, S. H. Oh, W. I. Cho, *Chem. Commun.* **2013**, *49*, 2004-2006.

[45] A. Viehbeck, M. J. Goldberg, C. A. Kovac, *J. Electrochem. Soc.* **1990**, *137*, 1460-1466.

[46] M. Walter, T. Zünd, M. V. Kovalenko, *Nanoscale* **2015**, *7*, 9158-9163.

[47] D. Wu, F. Jing, X. Xi, L. Ma, D. Lu, P. Yang, R. Liu, *J. Colloid Interface Sci.* **2019**, *538*, 597-604.